Advances in Environmental and Life Sciences 2 (2022) 18-31

Contents lists available at Egyptian Knowledge Bank

Advances in Environmental and Life Sciences

journal homepage: https://aels.journals.ekb.eg

Remediation of Iron (II) ions from wastewater using dicalcium phosphate chitosan composites

Abbas M Abbas*, Ayman Abd El-Moemen, Zineb M Anwar, Mohamed Zakaria

Department of Chemistry, Faculty of Science, Suez CanalUniversity,41522,Ismailia,Egypt

Abstract

Dicalcium phosphate (DCP) used as adsorbent and in presence of CS with different ratio to form dicalcium phosphate chitosan composites, (DCP-CS1) and (DCP-CS2) which were characterized by X-ray diffraction analysis (XRD), Fourier Transform Infra-red spectroscopy (FTIR), Scanning electron microscope together with energy dispersive X-ray (SEM with EDX) before and after removal. The findings revealed that DCP crystalline were mineralized in presence of CS and this confirmed that CS has a controlling role on the morphologies of DCP. Batch studies were conducted at initial Fe^{2+} ions concentration range of 50-250 mg/L ,100 mg of adsorbent dose, pH range centered around 4.9 and 70-minutes contact time at 25 ± 1 ^{o}C. The adsorption kinetics was well-described by the pseudo-second-order kinetic, the intraparticle diffusion model was not rate-limiting step and the adsorption isotherms were fitted with Langmuir and Freundlich models. The maximal adsorption capacities (q_m) for (DCP), (DCP-CS1) and (DCP-CS2) were 13.38, 14.96 and 19.79 mg g^{-1} for Fe^{2+} ions removal, respectively. Based on these findings, it can be concluded that DCP/CS composites can adsorb Fe^{2+} ions from aqueous solutions successfully due to functional groups such phosphate, hydroxyl and amino groups in its structure.

Keywords: Iron ions, Adsorption, Chitosan, Kinetics, Isotherms

1. Introduction

Water contamination by heavy metals (HMs) is a chronic global problem in all countries. HMs are immune and anti-degradable components transmitted by both natural and anthropogenic activities into water bodies. The crucial sources of anthropogenic waste are agricultural, industrial and domestic waste, that are growing owing to an increase in the global population [1].

Iron is one of the main water contaminants of many heavy metals (HMs). Iron occupies the 26th critical site in the periodic table, it is the 2^{nd} mostly common component on the globe, occurring in many forms in water [2]. Embedded iron can increase the efficacy of species that cause greater contamination of drinking water throughout the distribution system [3]. In water, iron piping can leak corroded iron, chlorine and whitening powder applied as a germicide to drinking water, oxidize and corrode iron. Iron is found in two types, soluble Fe^{2+} or in insoluble Fe^{3+}. Water containing Fe^{2+} ions is colorless and transparent owing to the total solubility ions in water. As soon as it is presented to the air, the water becomes turbid and starts to create a reddish-brown film. This residue is a form of iron oxidized that is not soluble in water [4]. The oxidation rates are not fast in aerated water and this reduced form will continue for some time when it has a pH less than 6.

The World Health Organization (WHO) limits the permissible concentration of Fe^{2+} ions in water to 0.3 mg/L. Excess Fe can cause illness such as Alzheimer, Arteriosclerosis, Diabetes mellitus, Cancer, Neurodegenerative diseases [5].

*Corresponding author.

Email address: abbasmamdoh@science.suez.edu.eg (Abbas M. Abbas)

doi 10.21608/AELS.2022.131623.1012

Received: 5 April 2022, Revised: 20 April 2022
Accepted: 23 April 2022: Published: 23 April 2022

For removing Fe^{2+} ions from waste water, several methods of separation can be used, including membranes [6], electrocoagulation [7], chemical precipitation [8], and ions exchange [9]. All these techniques have restrictions, including high costs, low extraction, highly energetic requirements, and waste disposal problems in some cases. In additionally, one of the most suitable treatment choices for treated water is adsorption. While adsorption is not a novel technique, recent advances in adsorbents have made it a far more efficient approach.

The usage of phosphate materials increased dramatically in recent years, primarily due to their high ability to extract a significant number of heavy metal ions when it contacts with the aqueous solutions. The resources of Calcium phosphates (CPs) have gained significant consideration in the field of treated water and toxic heavy metal extraction due to their environmentally benign characteristics and the high surface areas available [10].

Dicalcium phosphate anhydrate (DCPA, Monetite, $CaHPO_4$) was used as an adsorbent for Fe^{2+} ions uptake as a means of providing $PO_4{}^{3-}$group, higher surface area, preventing pollutant emission into the environment and relatively cheap. DCP has gained significant interest as among the most stable phases of dicalcium phosphates. Recently, several scientists have used monetite as an adsorptive for aqueous solution purification. Malathion extraction using monetite via aqueous solutions [11] Lately, efficient fluoride uptake from potable water by using DCP bundles has also been documented [12].

In addition, chitosan (CS) has gained great attention as an adsorbent in treated water applications, due to its abundance, antibacterial, biocompatibility, biodegradability, bioactivity, hydrophilicity, nontoxicity, and renewability [13]. Chitosan is a chitin that is N-deacetylated, a most common polymer on earth. The CS chemical name Poly-(1→4)-2-amino-2-deoxy-b-d-glucose [14], It gained considerable interest by using chitosan for extraction organic species ions and transition metal by adsorption process [15]. For its excellent binding ability, Chitosan chelates larger quantities of heavy metal than chitin, mainly owing to the free NH_2 groups exposed after chitin deacetylation. Also, it's soft and has a propensity to agglomerate or shape gel. It is partially soluble in diluted acids mineral including hydrochloric acid (HCl), phosphoric acid (H_3PO_4) and nitric acid (HNO_3) [16], it is also soluble in organic diluted acids including formic acid, acetic acid (HAc), etc. [17]. Several researchers have studied the efficacy of chitosan and its blends as an adsorption mechanism for heavy metal uptake, [18–20].

In this work, an effort was made to study the effect of chitosan (CS) on calcium phosphate (CPs) for removal of Fe^{2+} ions from wastewater. The specific objectives of this study are preparing crosslinking between dicalcium phosphate and chitosan (DCP /CS) for using as an adsorbent, characterization adsorbent by XRD, FTIR and SEM/EDX. The adsorption behavior of the Fe^{2+} ions removal on the adsorbent powder studied under conditions of adsorbent dose, pH, contact time, initial metal concentration, kinetics, and adsorption isotherm.

2. Material and method

2.1. Material

Analytical reagent grade of all chemicals used in this research. Iron sulfate heptahydrate and Chitosan Shrimp Shells, from LOBA CHEMIE, India. Glacial acetic acid 96% from El-Nasr Pharmaceutical Chemicals Co., Egypt. Hydrochloric acid (HCl, from Techno PharmChem, India. Sodium hydroxide solution 0.5 N (NaOH) and iron reagent (FerroVer Powder Pillows, 10 ml) from HACH Company, USA.

2.2. Method used for preparation of adsorbent powders

2.2.1. Dicalcium phosphate (DCP

Dicalcium phosphate (DCP) is used as adsorbent and a raw material in the recent study in preparation of dicalcium phosphate - Chitosan composite DCP–CS. Natural DCP dried in an oven at temperature of 80^oC for 24 h with the aim to eliminate moisture, dried DCP grinded in the agate mortar into a fine powder.

2.2.2. Dicalcium phosphate – chitosan composite (DCP-CS

• Composite 1: 10% Chitosan + 90% Dicalcium phosphate (DCP–CS1)

Disperse 1 gram of CS with a high-speed agitator in 50 ml of water and add 50 ml of 2% acetic acid while the agitation continues. Stir for 30 minutes or until dissolving is complete, then added 9 gm of DCP. Then, DCP – CS1 were performed using sonication method by stirring the solution with ultrasonic wave 42 kHz 130 W to 1 hours. After sonication processes, the mixture is placed into dishes and put in an oven to dried at 80 °C to 24 hours. Prior to characterization and use the dry solid was thinly milled into a fine powder.

• Composite 2: 30% Chitosan + 70% Dicalcium phosphate (DCP–CS2)

Disperse 3 gram of CS with a high-speed agitator in 50 ml of water and add 150 ml of 2% acetic acid while the agitation continues. Stir to 30 minutes or until dissolving is complete, then added 7 gm of DCP. Then, DCP–CS2 were performed using sonication method by stirring the solution with ultrasonic wave 42 kHz 130 W to 1 hours. After sonication processes, the mixture is placed into dishes and put in an oven to dried at 80 °C to 24 hours. Prior to characterization and use the dry solid was thinly milled into a fine powder.

2.3. Characterization

2.3.1. XRD Analysis

An XRD (The Bruker D8 Advance, Germany, using Cu anticathode ($\lambda_{CuK\alpha}$ = 1.5405Å), 40KV and 40mA) was used to evaluate the chemical composition phases and crystalline size of the various adsorbent powders. XRD patterns are recorded in 2-theta-scale ranges of 10°- 60° per a scan step of 0.02° and an acquire time of 9s per step. The phases obtained were identified by compared to the reference standards (JCPDS). The average crystalline size (D) of the obtained composite powders was estimated from XRD using the Scherrer formula [21] as seen below:

D = K λ **/ (**β **cos** θ**) (1)**

Where the average crystalline size is d, the wavelength X-ray is λ, Scherer's constant is k (0.92), the full width at half maximal (FWHM) intensity of a Bragg reflection is β and the Bragg's angle is θ.

2.3.2. FTIR Analysis

ATR-FTIR spectrometer (Bruker, Germany, Alpha-P), this device was equipped by ATR probe included a diamond crystal with a scan range up to 2 μm to identify the major chemical functional groups of the various samples prepared as well as the type of chemical bond between the various atoms in the groups. Sample powders was introduced to the crystal surface and then locked in prior to measurement with a "clutch – type" lever, each spectrum was recorded at 2 cm^{-1} resolutions with range 400 - 4,000 cm^{-1}.

2.3.3. SEM with EDX

Scanning Electron Microscopy (Joel, JSM-6360LA, Japan) equipped with EDX Unit, with accelerating voltage 30 KV, a magnification of 14x up to 1000000, was used to examine the surface morphology of the different adsorbent powders. The investigated samples were coated with a thin layer of pure gold before imaging using sputter coater. EDX analyzer was used to detect the chemical composition of the synthesized powders. The EDX system has a super ultra-thin window which means that it can analyze a wide range of elements.

2.4. Preparation of Fe^{2+} ion solutions

A Stock solution of Fe^{2+} ions 1000 ppm was prepared by dissolving a 4.978 g of $FeSO_4.7H_2O$ in 1 L distilled water, with resistivity of 18.2 Ω.cm at 25°C.

2.5. Adsorption studies

Batch adsorption experiments of 10 mL of 100 ppm Fe^{2+} ions solutions were performed. A predetermined quantity of adsorbent powders was transferred to the glass tubes and placed in stirred at maxiumum and ambient temperature (25 ± 1°C). As a control, a blank sample was used. After treatment, settling for 2 minutes and centerfuge using rotofix 32 A 4000 rpm to 5 minutes then filtration the supernate by syring filter 0.45 μm membrane then filtrate was analyzed for the Fe^{2+} ions concentration [22] by UV/Vis spectrometer a HACH

Lange-DR/6000 (Germany) [23] with 1,10 phenanthroline as reagent at wavelength 510 nm. Adsorption kinetics with a known quantity of adsorbent loading were investigated by varying the contact time from 0 to 100 minutes at (25 ± 1°C). Adsorption ability at equilibrium q_e (mg/g) and adsorption efficiency (% Removal) were evaluated as according to:

$$\mathbf{q_e = (C_o - C_e)\ V/\ m\ (2)}$$

$$\mathbf{\%\ Removal = [(C_o - C_e)\ /C_o\ ] \times 100\ (3)}$$

Where the initial concentration and equilibrium concentration of (Fe^{2+}) ions (mg/L) are C_o and C_e, the volume of solution (L) is V, the mass of the adsorbent material (g) is m.

3. Result and discussion

3.1. Characterization

3.1.1. XRD Analysis

An XRDpatterns of the DCP, DCP – CS1 and DCP–CS2 are presented in **Figure 1**. Adsorbents powder showed strong and sharp intensity of peaks at 2-theta angle =13.14°, 26.5°, 30.3°, 33° comparing to the valuation of ($CaPO_3(OH)$, Monetite – JCPD 09 – 008) [24, 25]. The crystal structure of DCP, monetite is tetrahedral representing the PO_4 group, the largest spheres is Ca atom, medium O atom, and smallest spheres H atom [26] and crystal system is Triclinic – Pinacoidal space group [27].

From previous studies the XRD of preparation chitosan (CS) gives two peaks at 2-Theta angle 10° and 20° [28]. The peak around 20° assigned to (CS) chain however, the crystalline structure of the chitosan (CS) was totally broken after removal Fe^{2+} ions on DCP–CS1 and DCP–CS2 that presented in **Figure 1**. By increasing the DCP/CS ratio, the peak of DCP, Monetite intensity steadily increased. The 2θ, crystal size, d-spacing (Å) and the main phase detected for adsorbents before removal showed in the **Table 1**.

PXRD of DCP, DCP–CS1 and DCP–CS2 that presented in **Figure 1** after Fe^{2+} ions removal did not reveal any new phases. Supported the idea that Fe^{2+} ions removal was not dependent on dissolution/precipitation mechanisms. Fe^{2+} ions uptake may be occurs using adsorption mechanisms such as surface complexation or ionic exchange [29].

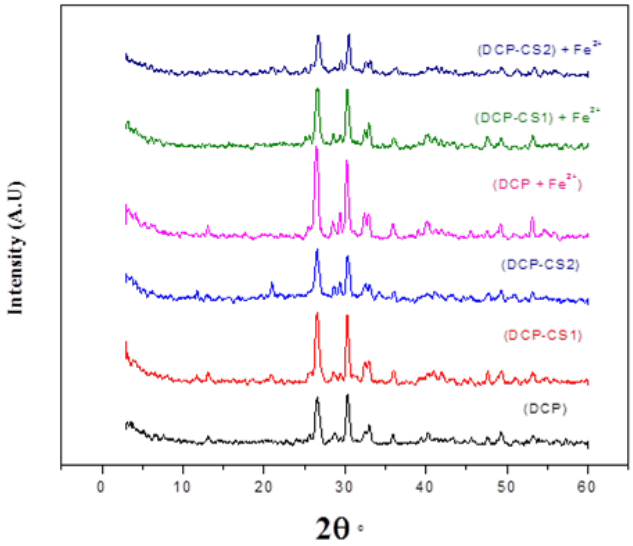

Figure 1: XRPD patterns of adsorbents before and after removal(Fe^{2+}) ions

PXRD showed some changes throughout their relative intensities and crystals sizes (**Table 2**). Also, there are also some little shifts in 2θ, d-spacing (Å) and crystals size (nm) of the maximal relative intensity (I/I^o) peak after Fe^{2+} ions uptake. this may be owing to the exchange of ions between Ca^{2+} and Fe^{2+} ions in lattice structure of adsorbents powder.

To calculate the values of average crystallite's size for all adsorbents before and after Fe^{2+} ion extraction from XRD data using Scherrer formula. Firstly, determine peak position and FWHM from XRD data. Then, put it in Scherrer equation for the calculation of crystallites size. Finally, determine the average crystallites size showed in the **S1**.

It is evident from all the data achieved shown in **S1** the average crystallites size (nm) of monetite (DCP) decrease after cross-linking with chitosan (CS). This suggested that in nature, the chitosan was amorphous [28]. Decreasing crystallinity caused an increase in the adsorptive of Fe^{2+} ions.

The average crystallites size of adsorbents increases after Fe^{2+} ions uptake. This may be related to the Fe^{2+} ions uptake depended not only on the substitution of Ca^{2+} with Fe^{2+} ions but also form complex compound on the surface of adsorbents, adsorption process influenced by adsorbent ability to bond with Fe^{2+} ions that comes from either DCP or CS active sites. therefore, Fe^{2+} ions are ca-

Table 1: 2θ,d-spacing (Å), crystal size (nm)at the maximal relative intensity (I/I^o) peak and the main phasedetected for the prepared adsorbents.

Character	2θ	d-spacing (Å)	Crystal size (nm)	Main phase detected
DCP	30.30	2.95	33.60	Monetite
(DCP – CS1)	30.27	2.95	45.00	Monetite
(DCP – CS2)	26.52	3.36	18.80	Monetite

Table 2: 2: 2θ, d-spacing (Å), crystal size (nm)at the maximal relative intensity (I/I^o) peak after (Fe^{2+})ions removal.

Character	2θ	d-spacing (Ao)	Crystal size (nm)
(DCP) + Fe^{2+}	30.23	2.95	38.30
(DCP –CS1) + Fe^{2+}	26.64	3.34	22.60
(DCP –CS2) + Fe^{2+}	30.47	2.93	33.70

pable of forming a bond with chitosan NH_2 group to form a complex compound chelate [chitosan - Fe^{2+}] [30].

3.1.2. *FTIR Analysis*

The FT-IR measurements of DCP, DCP-CS1 and DCP-CS2 powder is represented in **Figure 2**, The wavenumbers and corresponding assignments are represented in **Table 3** before removal Fe^{2+} ions.

By insertion and interactions of the CS inside the DCP network with different ratio to form composites DCP-CS, the FT-IR spectrum of DCP after insert CS. As it can be seen **Figure 2**, Some decreases in the intensity of the characteristic peaks of DCP, belong to P-O stretching, and the peaks belong to (P)O–H stretching, suggest that the (PO_4^{3-}) groups are the main active sites, when cross-linking with CS.

The study found that the charged functional groups existing on the composites surface, (-NH_2) groups or C=O groups of CS, act as nucleation centers for calcium phosphate particles. Firstly, a layer of Ca^{2+} ions formed with CS, and it was strongly bound to C=O groups and (-NH_2) groups of CS. Secondly, by electrostatic interaction, another layer of (PO_4^{3-}) ions was attracted to the Ca^{2+} ions layer.

It is evident from all the data achieved shown in **Figure 2** and **S2**. The result of FT-IR spectrum showed that there are no new absorption peaks were detected, there are alittle peak shifts which may be attributed to the corporation and substitution of Fe^{2+} ions in the lattice structure of DCP, DCP-CS1 and DCP-CS2.

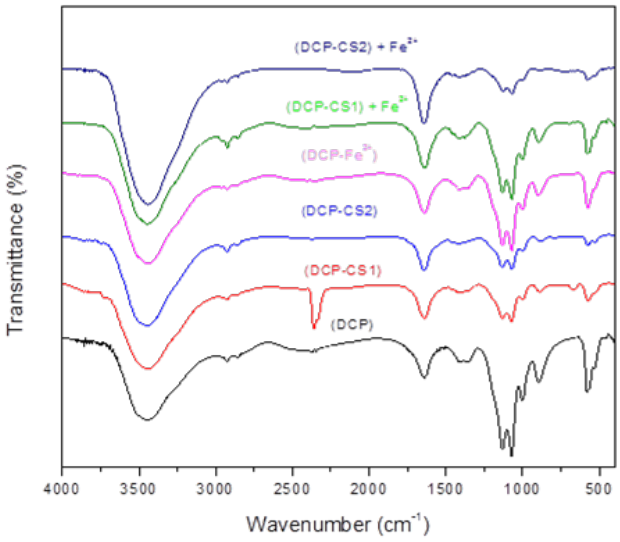

Figure 2: FT-IR spectra of DCP, DCP-CS1 and DCP-CS2 powder before andafter removal Fe^{2+} ions

3.1.3. *Scanning Electron Microscope (SEM and Energy Dispersive Analysis X-ray (EDX*

SEM images at 500× and 1000× magnification of DCP show the typical morphology expected for monetite (i.e. a rectangular, plate-like crystal [33], By insertion and interactions of the CS inside the DCP network with different ratio to form composites DCP-CS1 and DCP-CS2, SEM images of DCP

Table 3: IR spectra (cm^{-1}) and assignments foradsorbents before removal (Fe^{2+}) ions.

(DCP)	(DCP-CS1)	(DCP-CS2)	Assignments	Ref.
3448.79	3447.82	3450.11	O–H stretching of residual free water	[31]
2924.86 2854.12	2926.56 2857.49	2926.08 2856.66	(P) O–H stretching	[31]
2371.27	2360.34	2370.07		
1638.52	1630	1630	H –O–H bending and rotation of residual free water	[32]
-	1638.62	1642.08	C= O stretching of amide I	[32]
-	1418.19	1416.26	Amino II (-NH_2)	[32]
1131.85 1070.86	1131.58 1072.50	1133.11 1070.48	P–O stretching	[32]
1000.77	1002.14	998.33		
894.88	889.22	879.42	P–O(H) stretching	[32]
580.64 533.65	574.67 532	575.85 529.232	O–P–O(H) bending mode	[32]

after insert CS were similar but the crystals appeared to have a lowered aspect ratio and composed of smaller, thicker crystallites, showed a similar morphology to one another but different and distinct from the first sample; these powders reveal a general granular morphology with regular shaped crystalline components found. The morphological variations are most likely attributable to changes in the CS contents used in synthesis [32] are presented in **S3,4**.

The polymer network regulated the production of calcium phosphate in polymeric solution, according to SEM results of DCP-CS composites. The smaller the crystal of the inorganic phase produced, the larger the amount of polymer required. This might be due to increased contact between the crystals of calcium phosphate and polymer, which could restrict growth of calcium phosphate crystal with solution of chitosan [32].

Energy dispersive X-ray (EDX) was used to determine the elemental composition of the all-adsorbent powder. The average Ca/P ratio was 1.60 in DCP, 1.65 in DCP-CS1, and 1.78 in DCP-CS2 powders. These values are greater than the value of 1.0 for stoichiometric monetite [34].

SEM of DCP, DCP–CS1 and DCP–CS2 after Fe^{2+} ions uptake revealed some changes in morphology and microstructure. EDX results indicated the presence of (Fe^{2+}) ions with all adsorbents. The weight and atomic percentage of Ca^{2+} ions and $PO_4{}^{3-}$ in all adsorbents after metal ion uptake was less than its value before metal ion removal as shown in **S5-7**.

3.2. Optimal condition studies

3.2.1. Effect of adsorbent dose

Impact of changing dosage powders on the Fe^{2+} ions removal at C_0=100 mg/L, adsorbent dose of 20, 40, 60, 80 and 100 mg, pH = 4.90, Temperature 25±1^{o}C at 120 minutes for both DCP and DCP–CS1 and 60 minutes for DCP–CS2 were investigated, and the findings obtained are seen in **S8**. The uptake percent (%) of Fe^{2+} ions from solution increased, while the adsorption ability decreased. This occurred when the dose of adsorbent was increased **(S9-11)**. The effective sites on the surface of adsorbent increase with increasing adsorbent content, and then it provides more adsorption sites to adsorb, leading to increased Fe^{2+} ions removal. The decrease in the capacity of adsorption could be owing to an interaction between binding sites and the higher adsorbed dose or Fe^{2+} ions deficiency in the solution with respect to the binding sites present [25].

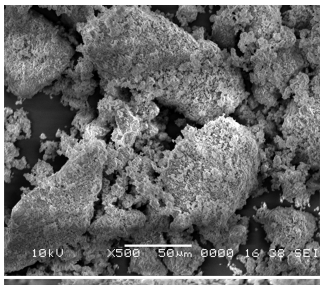

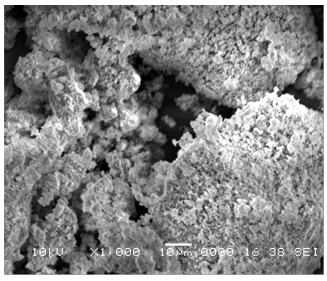

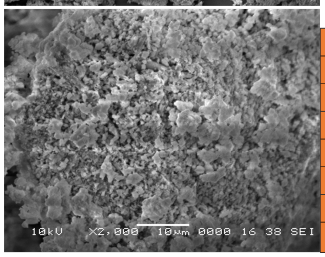

Element	Wt %	At %
C K	5.22	10.05
N K	3.17	3.19
O K	29.10	45.02
Na K	0.46	0.49
P K	19.44	15.54
Ca K	42.61	25.71
Total	100	100

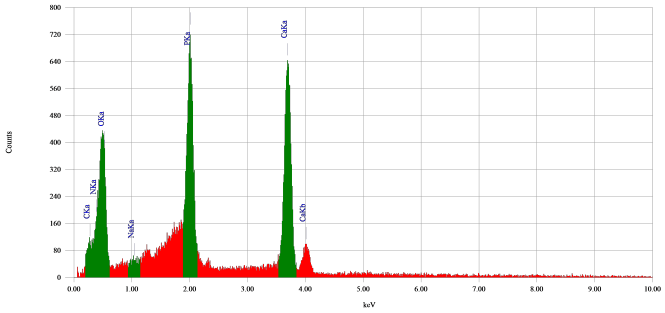

Figure 3: SEM images and EDX analysis of DCP-CS1

3.2.2. *Effect of Contact Time*

The contact time in almost all the adsorption systems could always be viewed as an essential parameter. In that research, 100 mg of all the adsorbents were agitated separately at ambient temperature with 10 mL of 50 mg/L Fe^{2+} ions solutions for different exposure periods 1-100 min. The observed findings were presented in **S12-15**.

At certain periods of time (q_t), the quantity of Fe^{2+} ions adsorbed per unit of weight the adsorbents were determined. The adsorption of Fe^{2+} ions increased with time and equilibrium was reached within 1-70 min. The results proved that increasing in contact time does not affect on the Fe^{2+} ions uptake. Even though the time of contact was variable for three adsorbents, adsorption seems to be achievable within 70 minutes for all adsorbents. As seen in Figures, DCP-CS2 demonstrated greater Fe^{2+} ions adsorption ability and adsorption efficiency (% Removal) compared to DCP and DCP–CS1. In the presence of all adsorbents, reaching rapid adsorption equilibrium specifically indicates that a high number of reaction active sites are available on DCP and CS for Fe^{2+} ions uptake.

3.2.3. *Effect of pH*

The impact of pH was observed, differing levels the pH of solution from 1.0 to 7.0 with the initial Fe^{2+} ions concentration of 50 mg/L. The findings demonstrate that the adsorption was carried out at original pH solution for Fe^{2+} ion (pH range 4.90). This is for following reasons: In acidic medium, adsorbent DCP [35] and CS dissolves in the solution [17]. In basic medium, iron precipitates in the form of ferrous hydroxide [36].

3.2.4. *Effect of initial Fe^{2+} ions concentration*

The impact of the initial Fe^{2+} ions concentration on the rate of adsorption was analyzed using constant weight 100 mg of adsorbents DCP, DCP–CS1 and DCP– CS2 at temperature 25 ± 1^{o}C and pH 4.9 using different concentrations of Fe^{2+} ions ranging between 25 to 250 mg/L. The findings are given in **S16-19**.

They demonstrate that the percent of Fe^{2+} ions adsorption increasing by decreasing the Fe^{2+} ions initial concentration. This result indicates that a strong connection between DCP and CS toward Fe^{2+} ions.

3.3. *Adsorption kinetics*

Kinetic experiment is useful in assessing the capability of adsorption, that is very significant in modeling and designing the mechanism of adsorption [37]. pseudo-first-rate equation, pseudo-second-order model and intra-particle diffusion models to analyze the control method of the adsorption process, including the physical adsorption, mass transfer, and chemical reaction.

a. pseudo first-order model:

Express the linear form as:

$$\mathbf{\ln (q_e - q_t) = \ln q_e - k_1\ t} \quad \textbf{(4)}$$

where q_t is the amount of adsorbed (Fe^{2+}) ions (mg g^{-1}) at time (t), q_e is the maximal ability of adsorption (at equilibrium) (mg g^{-1}) and k_1(min^{-1})

is the constant rate. Adsorption kinetics evaluated at initial (Fe^{2+}) ions concentration of 50 mg/L, pH=4.9, dosage of adsorbent 100 mg/10 mL at 25±1^{o}C. The ln (q_e-q_t) vs t diagram was drawn as can be seen in **S20**.

Equilibrium rate constant (k_1) and regression coefficient (R^2) estimated for all adsorbents from the plots of the pseudo-first-rate equation of uptake (Fe^{2+}) ions at equilibrium (q_e) are indicated in (Table 15). As it can be seen in **S20** and **S21**, the regression coefficient (R^2) does not close toward unity. Also, the results of q_e studies evaluating from pseudo-first-rate equation for all adsorbents are different and not correspond directly to the experimental q_e result.

b. pseudo-second-order model:

Express the linear form as:

$$\mathbf{t/q_t = 1/k_2 q_e^2 + t/q_e} \quad \textbf{(5)}$$

where q_t is the amount of adsorbed (Fe^{2+}) ions (mg g^{-1}) at time (t), q_e is the maximal ability of adsorption at equilibrium (mg g^{-1}) and k_2 (g mg^{-1} min^{-1}) is the constant rate for the second order. The k_2 and q_e values were determined from plotting of t/q_t versus t for second-order reactions (**Figure 4**) using the intercept and slope values as summarized in **S21**.

Constant rate (k_2) and regression coefficient (R^2) estimated from the plotting of pseudo-second-rate equation of uptake Fe^{2+} ions, pH=4.9 at equilibrium, (q_e) for all adsorbents are given in **S21**. from linear plots, the $\mathbf{q}_{e,\,experimental}$ and the $\mathbf{q}_{\,e,\,calculated}$ values are very close to each other, and also, the calculated coefficients of determination(R^2), are also very close to unity.

4. Weber-Morris intraparticle diffusion model:

Fitting an intra-particle diffusion plot is the most widely used technique for classify the adsorption mechanism. The amount of Fe^{2+} ions adsorbed (q_t) at time (t), was plotted against the square root of t ($t^{1/2}$), according to Eq. proposed by Weber and Morris as follows [38]:

$$\mathbf{Q_t = K_{id}\, t^{0.5} + C} \quad \textbf{(6)}$$

where C is thickness double-layer and k_{id} is constant of diffusion rate (mg/g $min^{1/2}$), q_t is the Fe^{2+} ions adsorbed at a time (mg/g), t is the time (min). Two straight lines with different slopes were observed due to the differing magnitude of adsorption in the initial and final stages of the experiment (**Figure 5**).

In the q_t vs. $t^{0.5}$plot, the two regions indicate that the sorption process continues by surface sorption and intra-particle diffusion. The initial fast uptake can be because of the boundary layer (film diffusion). The intraparticle diffusion or pore diffusion starts after the outer surface loading has been completed. The second linear component of the plot shown in **Figure 5** refers to the transport of Fe^{2+} ions within particles DCP, DCP-CS1 and DCP - CS2 [39]. The slope of the second linear portion of the plot has been defined to yield the intraparticle diffusion, parameter of k_{i1}, ${R_{i1}}^2$ (first stage) and k_{i2}, ${R_{i2}}^2$ (second stage) are listed in **Table 4**. On the other side, the intercept give an indication about the thikness of boundary layer effect [40]. In the rate-control process, the greater the intercept C, the greater the surface sorption contribution [41].

The plot revealed, as shown in **Figure 5**, that the intraparticle diffusion isn't the phase of rate-limiting step because it did not pass through the origin [39]. In comparison, the first straight portion is referred to a macropore diffusion process and the second linear portion can also be referred to a micropore diffusion process [42]. Moreover, the first stage is faster than the second one. This action can be associated with the very slow diffusion from the surface film of the adsorbate into the micropores, the lowest available adsorption sites [40].

It is evident from all the data achieved shown in **S20, Figures 4 and S21**, the adsorption process was considered to be best suited to the pseudo-second-order kinetic based on the regression coefficient (R^2) for all adsorbents are very nearly to unity, which is larger than the pseudo-first-order model. Moreover, $\mathbf{q_e}$(calculated)were quite similar to $\mathbf{q}_{\,e}$,(experimental) meaning that chemisorption involves valence forces by exchange electrons between the sorbent and sorbate may be the rate-limiting. Also, on two sorption sites on the sorbent surface, only one metal ion is sorbed [42].

From **Table 4**, this can be conclouded that Fe^{2+} ions (pH=4.9), adsorption onto DCP, DCP–CS1 and DCP–CS2, the values obtained of k_{i1} were greater

Table 4: Intraparticlediffusion model parameters for Fe^{2+} ions(pH=4.9), adsorbed on DCP, DCP–CS1 and DCP–CS2

Intraparticle diffusion model	K_{i1} (mg/g $m^{0.5}$)	K_{i2} (mg/g $m^{0.5}$)	$R_{i1}{}^2$	$R_{i2}{}^2$	Intercept $_{i1}$	Intercept $_{i2}$
DCP	0.75464	0.09834	0.98072	0.74269	0.27082	3.88468
(DCP – CS1)	0.78021	0.10706	0.9396	0.76736	0.54006	3.84887
(DCP – CS2)	0.89096	0.10438	0.93356	0.95655	0.88769	4.02108

Table 5: Isothermparameters and regression coefficient (R^2) calculated for theadsorption of Fe^{2+} using DCP, DCP–C1 and DCP–CS2.

Adsorbent	Langmuir Isotherm				Freundlich Isotherm			
	q_{max}(mg/g)	K_L	R_L	R^2	K_F	1/n	n	R^2
DCP	13.3850	0.1560	0.0535 to 0.8501	0.9782	2.9754	0.33173	3.0144	0.8828
(DCP – CS1)	14.9611	0.1498	0.0616 to 0.9014	0.9782	3.2600	0.3409	2.9328	0.94273
(DCP – CS2)	19.7941	0.2044	0.0699 to 0.9550	0.9870	4.3643	0.3787	2.6401	0.9783

than those of k_{i2}. That clarification may be of pore blockage as circumscription of the available vacant space for diffusion in them.

Actually, the above three models could explain the proposed sorption process to a definit extend, but during the first minutes of the process, they could not predict the high adsorption rate. External mass transfer or surface diffusion most likely controlled the initial stages, followed by chemical reaction or a constant-rate stage, and diffusion producing a progressive drop in the process rate [42].

4.1. Adsorption isotherm studies

Adsorption isothermal studies are necessary for illustrating the adsorption process at equilibrium conditions. The isotherm of adsorption is defined by certain constants that represent the adsorbent's affinity and can also be used to detect the ability of adsorption. The adsorption of Fe^{2+} ions from polluted water using DCP, DCP–CS1 and DCP–CS2 is thought to follow the isothermal adsorption model, where the adsorbate maintains a dynamic equilibrium between the adsorpation and desorption at constant temperature [43, 44].

In order to express the quantitative relationship between the degree of sorption and the residual solute concentration, two most commonly used mathematical models were adopted: Langmuir and Freundlich adsorption isotherms.

Langmuir isotherm assumes adsorabate monolayer coverage over the ahomogeneous adsorbent surface and the adsorption to the surface of each molecule has the same adsorption activation energy.

Freundlich isotherms conclude that with the possibility of multilayer adsorption, aheterogeneous surface with anon-uniform distribution of adsorption heat over the surface [43, 45].

The maximal (Fe^{2+}) ions adsorption capacities were evaluated by analyzing the experimental data onto DCP, DCP–CS1 and DCP–CS2, as they provide the greater removal efficiency. The data of Fe^{2+} ions adsorption by DCP, DCP–CS1 and DCP–CS2 were examined in accordance with langmiur adsorption isotherm whose linearized equation was:

$$\mathbf{C_e/q_e = C_e/q_m + 1/ K_L q_m} \quad \mathbf{(7)}$$

where q_m (mg /g) and K_L (L /mg) are constants in Langmuir's equation which are referred to the maximal adsorption capacity. Also q_e and C_e parameters represent the equilibrium adsorption capacity and the equilibrium concentration Fe^{2+} ions that is remaining in solution, respectively. q_e was determined as follows:

$$\mathbf{q_e = ((C_o - C_e)\, V) / m} \quad \mathbf{(8)}$$

Where the initial concentration and equilibrium concentration of Fe^{2+} ions (mg/L) are C_o and C_e,

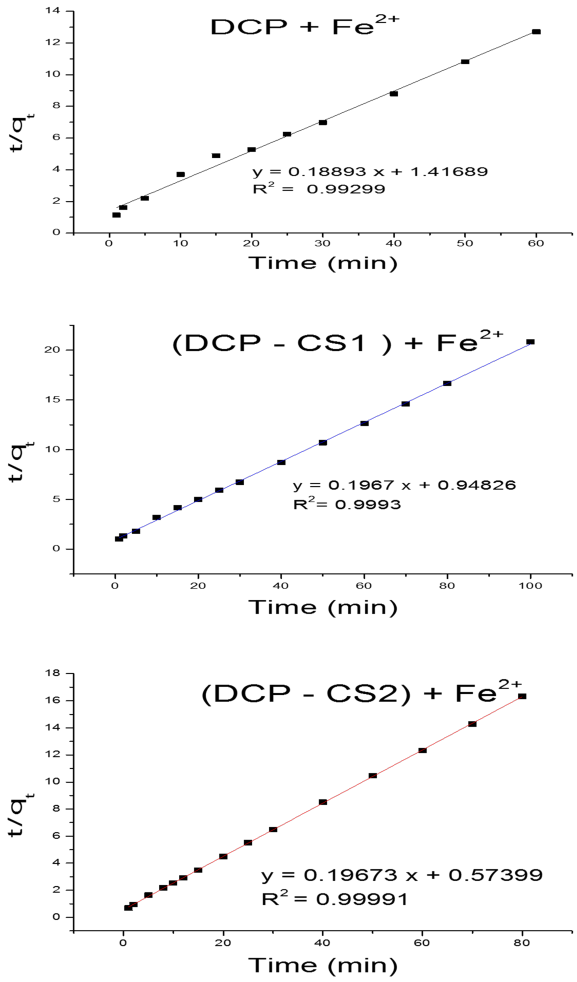

Figure 4: Pseudo -second-order of Fe^{2+} ions (pH=4.9), adsorbed on DCP, DCP–CS1 andDCP–CS2 at conditions of 50 mg/L metal ions concentration, adsorbent mass 100mg/10 mL at 25±1^{o}C

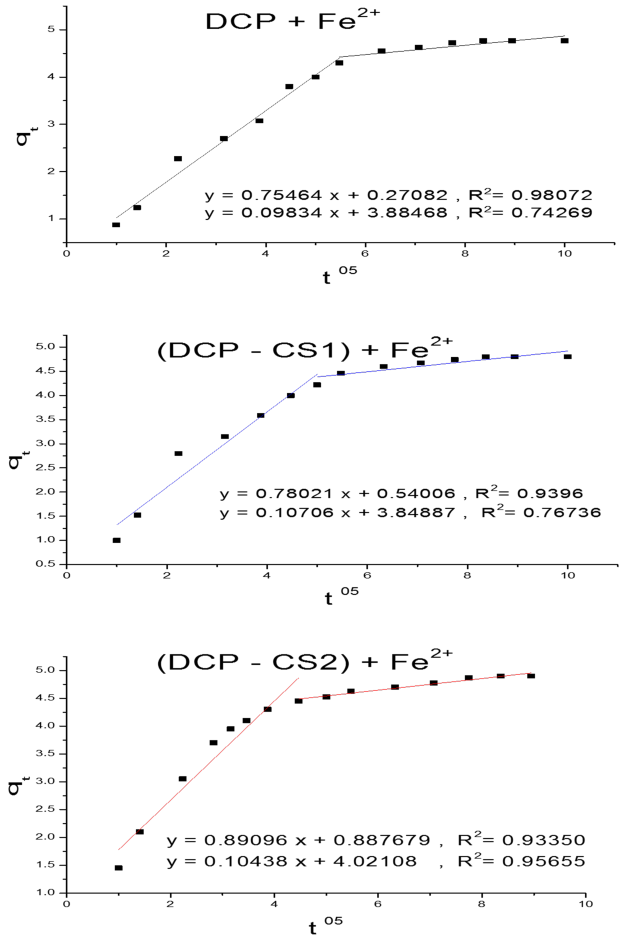

Figure 5: Intra-particle diffusion plot of Fe^{2+} ions (pH=4.9), adsorbed on DCP, DCP–CS1 and DCP–CS2 at conditions of 50 mg/Lmetal ions concentration, adsorbent mass 100 mg/10 mL at 25±1^{o}C

the volume of solution (L) is V, the mass of the adsorbent material (g) is m.

A plot of C_e/q_e vs. C_e (**Figure 6**) gives a linear trace with a slope of $1/q_m$ and intercept of $1/K_L q_m$. On the basis of separation factor, R_L, given by a further analysis of the Langmuir equation can be performed.

$$\mathbf{R_L = 1/(1 + K_L C_e)} \quad \mathbf{(9)}$$

Where C_e is a concentration of the solution at which adsorption is carried out in the equilibrium liquid phase, when (R_L)value lies between 0 and 1 is favorable adsorption, while $R_L > 1$ is unfavorable adsorption, and R_L=1 is linear adsorption, while the adsorption process is irreversible if R_L= 0 [45].

The findings gained was also analyzed in accordance with the Freundlich equation represented as:

$$\mathbf{q_e = \log K_F C_e^{1/n}} \quad \mathbf{(10)}$$

Express the linear form as:

$$\mathbf{\log q_e = \log K_F + (1/n) \log C_e} \quad \mathbf{(11)}$$

While q_e is the amount adsorbed (mg/g), C_e is the adsorbate equilibrium concentration (mg/L) and Freundlich adsorption ability and adsorption intensity constants, respectively are K_F and n.

A log q_e vs. log C_e plot (**Figure 7**) gives a linear trace with 1/n slope and log K_F intercept. The (1/n) value in the range of (0 and 1) is a predicting of adsorption intensity of (Fe^{2+}) ions onto the adsorbent and the type of isotherm to be irreversible

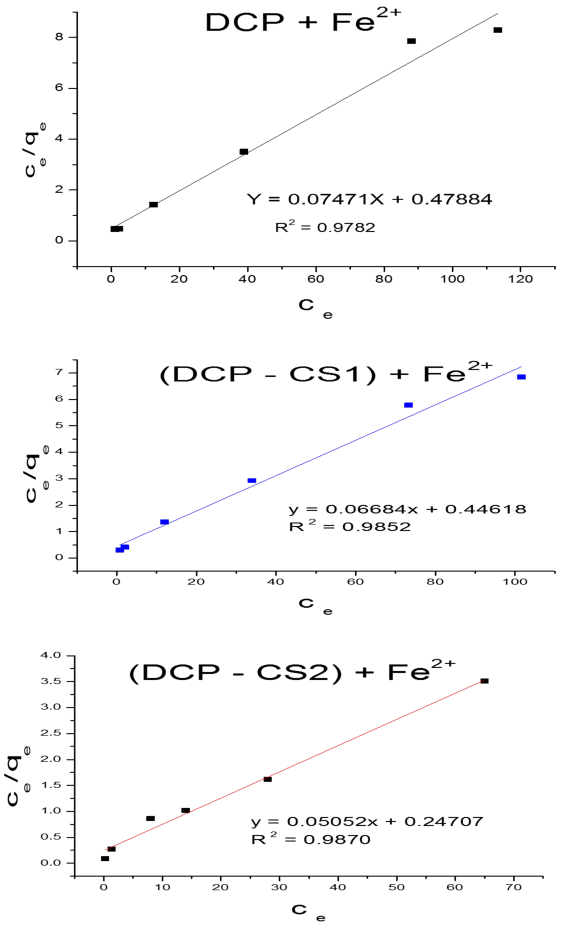

Figure 6: Langmuir for Fe^{2+} ions adsorbed on DCP, DCP–CS1 and DCP–CS2at conditions of 50-250 mg/L Fe^{2+} ionsconcentration, mass 100 mg/10 mL at 25±1^{o}C.

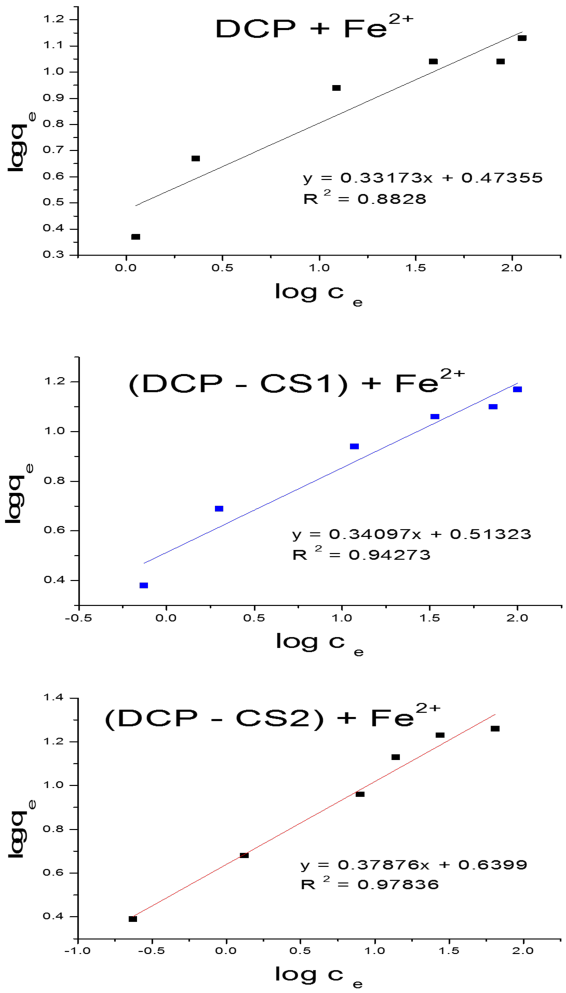

Figure 7: Freundlish for Fe^{2+} ions adsorbed on DCP, DCP–CS1 and DCP–CS2 at conditions of 50-250 mg/L Fe^{2+} ions concentration, mass 100 mg/10 mL at 25±1^{o}C

(1/n=0), favourable (0<1/n<1) and unfavourable (1/n >1) [45], The value of (1/n) describes the heterogeneity of the surface, becoming more heterogeneous as its value reaches 0. the value of n shows the degree of nonlinearity between the concentration of the solution and the adsorption: if (n =1), is linear adsorption; if (n <1), adsorption is a chemical process; if (n > 1), then adsorption is a physical process [46, 47].

The isotherm parameters and regression coefficient (R^2) measured for the adsorption of (Fe^{2+}) ionsusing DCP, DCP–CS1 and DCP–CS2 are listed in **Table 5**.

Adsorption of Fe^{2+} ions on surface of adsorbents DCP, DCP–CS1 and DCP–CS2 follow Langmuir and Freundlich isotherms.The Langmuir monolayer adsorption capacity obtained from this study is 13.38, 14.96 and 19.79 mg/g at 25±1^{o}C for DCP, DCP–CS1 and DCP–CS2, respectivitely. The result of dimensionless separation factor (R_L) for adsorbents is between 0 and 1, indicated that of Fe^{2+} ions adsorption onto DCP, DCP–CS1 and DCP–CS2 is favorable.

Freundlich parameter (1/n) obtained from the plot (**Figure 6,7**) falls between (0 and 1), value of (n > 1) suggests the physical adsorption of Fe^{2+} ions onto DCP, DCP–CS1 and DCP–CS2.

Table 6: Comparisons with previous works

adsorbent	Removal efficiency	Optimum condition for removal	Ref.
DCP	95% 475 mg/1 g of adsorbent	C_0=50 mg/L, dose= 0.1g, pH=4.9, 70 min	This work
DCP-CS1	96% 480 mg/1 g of adsorbent		
DCP-CS2	98% 490 mg/1 g of adsorbent		
Zeolite Y	98% 0.25 mg/1 g of adsorbent	C_0=1.15 mg/L, dose= 4.5g, pH=6.5, 60 min	[48]
Rice Husk Ash	98% 11.7 mg/1 g of adsorbent	C_0=20 mg/L, dose= 0.6 g, pH=5, 60 min	[49]
Chitosan	100% 25 mg/1 g of adsorbent	C_0=55 mg/L, dose= 2.07 g, pH=3-4, 360 min	[50]
Activated Carbon from Olive Stones by Microwave	97.99% 78 mg/1 g of adsorbent	C_0=20 mg/L, dose= 0.25 g, pH=4.5, 3 h	[54]
Activated Carbon from Olive Stones by Conventional Heating	97.99% 64 mg/1 g of adsorbent	C_0=20 mg/L, dose= 0.3 g, pH=4.5, 3 h	
Activated Carbon Prepared from Coconut Shell	88.07 % 14.5 mg/1 g of adsorbent	C_0=16.6 mg/L, dose= 1 g, pH=6, 80 min	[51]
Activated Biochar of Colocasia esculenta	72.96% 1.5 mg/1 g of adsorbent	C_0=3 mg/L, dose= 1.5 g, pH=7.75, 180 min	[52]
Granular activated carbon	99.02% 5 mg/1 g of adsorbent	C_0=10 mg/L, dose= 2 g, pH=5, 10 min	[55]
Amberlite IR-120H	99.42% 5 mg/1 g of adsorbent		
Pomegranate peel carbon	100% 67 mg/1 g of adsorbent	C_0=20 mg/L, dose= 0.3 g, pH=5-6, 40 min	[53]

5. Conclusions

Here, dicalcium phosphate (DCP) and dicalcium phosphate-chitosan composites DCP–CS1 and DCP–CS2 are characterized by XRD and EDX-SEM and then used as adsorbents for Fe^{2+} ions uptake from waste water. The maximal uptake efficiency for adsorbents at a range of pH=4.9 at contact time 70 min. with 50 mg $L^{-1}Fe^{2+}$ ions concentration. Adsorption of Fe^{2+} ions onto adsorbents tends to follow second-order kinetics with a high correlation factor and the mechanism of adsorption was chemisorption. The adsorption of Fe^{2+} ions on surface of DCP, DCP–CS1 and DCP–CS2 follow Langmuir and Freundlich adsorption isotherm, the adsorption is physical in nature and the maximal adsorption capacity was found to be 13.38, 14.96 and 19.79 mg g^{-1} (at 25 ± 1^{o}C), respectively. Finally, study the effect of chitosan on calcium phosphate showed that adsorbents can adsorb Fe^{2+} ions successfully due to having functional groups such

as phosphate, hydroxyl and amino groups in its structure.

References

[1] M. E. Goher, M. H. H. Ali, S. M. El-Sayed, Heavy metals contents in Nasser Lake and the Nile River, Egypt: An overview, Egypt. J. Aquat. Res 45 (4) (2019) 301–312.

[2] N. Khatri, S. Tyagi, D. M. Phd, Recent strategies for the removal of iron from water: A review, J. Water Process Eng 19 (2017) 291–304.

[3] J. D. Navratil, M. T. S. Tsair, Magnetic separation of iron and heavy metals from water, Water Sci. Technol. J. Int. Assoc. Water Pollut. Res 47 (1) (2003) 29–32.

[4] P. Q. Governor, D. T. Arnold. [link].
URL http://www.dph.illinois.gov/search/site/iron

[5] R. B. Hernández, Coordination study of chitosan and Fe3+, J. Mol. Struct 877 (1) (2008) 89–99.

[6] S. Alzahrani, A. W. Mohammad, N. Hilal, P. Abdullah, O. Jaafar, Comparative study of NF and RO membranes in the treatment of produced water-Part I: Assessing water quality, Desalination 315 (2013) 18–26.

[7] S. Vasudevan, J. Jayaraj, L. Jothinathan, G. Sozhan, Removal of iron from drinking water by electrocoagulation: Adsorption and kinetics studies, Korean J. Chem. Eng. - KOREAN J CHEM ENG 26 (2009) 1058–1064.

[8] D. F. Morosini, C. A. M. Baltar, A. C. Duarte-Coelho, Iron removal by precipitate flotation, Rem Rev. Esc. Minas 67 (2) (2014) 203–207.

[9] Z. F. Pan, L. An, Removal of Heavy Metal from Wastewater Using Ion Exchange Membranes, Applications of Ion Exchange Materials in the Environment, Inamuddin (2019) 25–46.

[10] T. T. T. L. Hoang, F. Unob, S. Suvokhiaw, N. Sukpirom, One-pot synthesis of amorphous calcium phosphate/Fe3O4 composites and the application in the removal of cadmium, J. Environ. Chem. Eng 8 (2) (2020) 103653–103653.

[11] M. M. Mirković, Adsorption of malathion on mesoporous monetite obtained by mechanochemical treatment of brushite, RSC Adv 6 (15) (2016) 12219–12225.

[12] C. Shen, Efficient removal of fluoride from drinking water using well-dispersed monetite bundles inlaid in chitosan beads, Chem. Eng. J 303 (2016) 391–400.

[13] A. R. Kaveeshwar, M. Sanders, S. K. Ponnusamy, D. Depan, R. Subramaniam, Chitosan as a biosorbent for adsorption of iron (II) from fracking wastewater, Polym. Adv. Technol 29 (2) (2018) 961–969.

[14] M. W. Wan, C. C. Kan, B. Rogel, M. Dalida, Adsorption of copper (II) and lead (II) ions from aqueous solution on chitosan-coated sand, Carbohydr. Polym 80 (2010) 891–899.

[15] G. Annadurai, L. Y. Ling, J. F. Lee, Adsorption of reactive dye from an aqueous solution by chitosan: isotherm, kinetic and thermodynamic analysis, J. Hazard. Mater 152 (1) (2008) 337–346.

[16] O. Gylienė, S. Višniakova, Heavy Metal Removal from Solutions Using Natural and Synthetic Sorbents, Environ. Res. Eng. Manag 43 (1) (2008) 28–34.

[17] A. H. Chen, S. C. Liu, C. Y. Chen, C. Y. Chen, Zn (II), and Pb (II) ions in aqueous solution on the crosslinked chitosan with epichlorohydrin, J. Hazard. Mater 154 (1-3) (2008) 184–191.

[18] S. R. Akaji, D. Dewez, Functionalized Glutathione on Chitosan-Genipin Cross-Linked Beads Used for the Removal of Trace Metals from Water, International Journal of Biomaterials (2020).

[19] A. A. Menazea, Chitosan/graphene oxide composite as an effective removal of Ni, Cu, As, Cd and Pb from wastewater, Comput. Theor. Chem 1189 (2020) 112980–112980.

[20] J. Weißpflog, Solubility and Selectivity Effects of the Anion on the Adsorption of Different Heavy Metal Ions onto Chitosan, Molecules 25 (11) (2020).

[21] A. L. Patterson, The Scherrer Formula for X-Ray Particle Size Determination, Phys. Rev 56 (10) (1939) 978–982.

[22] A. D. Eaton, American Water Works Association, and Water Environment Federation, Standard methods for the examination of water and wastewater, American Public Health Association, Washington, D.C., 2005.

[23] E. Carré, J. Pérot, V. Jauzein, L. Lin, M. Lopez-Ferber, Estimation of water quality by UV/Vis spectrometry in the framework of treated wastewater reuse, Water Sci. Technol 76 (2017) 2017096–2017096.

[24] L. P. Higuita, A. F. Vargas, M. J. Gil, L. F. Giraldo, Synthesis and characterization of nanocomposite based on hydroxyapatite and monetite, Mater. Lett C (175) (2016) 169–172.

[25] H. Saghatchi, R. Ansari, H. Z. Mousavi, Highly efficient adsorptive removal of uranyl ions from aqueous solutions using dicalcium phosphate nanoparticles as a superabsorbent, Nucl. Eng. Technol 50 (7) (2018) 1112–1119.

[26] R. T. Downs, M. Hall-Wallace, The American Mineralogist crystal structure database, Am. Mineral 88 (1) (2003) 247–250.

[27] S. D. Poštić, X-Ray Diffraction Technique in the Analysis of Phases of Hydroxylapatite and Calcium Phosphate in a Human Jaw, Int J BioMed 4 (2) (2014) 109–113.

[28] G. M. Elkady, H. Fathallah, M. Elfadl, M. Elsayed, A. Selim, REMOVAL OF FE (II) AND MN (II) FROM WASTEWATER USING NANO-CHITOSAN PREPARED FROM SHRIMP WASTE, Al-Azhar Bull. Sci 28 (2017) 45–56.

[29] E. Mavropoulos, N. Rocha, M. H. Rocha-Leão, M. Silva, A. Rossi, Heavy Metals Immobilization by Hydroxyapatite-Alginate Composite in Simulated Gastric Fluid, Key Eng. Mater. - KEY ENG MAT (2008) 467–470.

[30] Y. Wang, B. Li, Y. Zhou, D. Jia, In Situ Mineralization of Magnetite Nanoparticles in Chitosan Hydrogel, Nanoscale Res. Lett 4 (9) (2009) 1041–1046.

[31] M. S. Djošić, Electrochemical synthesis of nanosized monetite powder and its electrophoretic deposition on titanium, Colloids Surf. Physicochem. Eng. Asp 341 (1) (2009) 110–117.
[32] K. H. Park, S. J. Kim, W. Y. Lee, H. J. Song, Y. J. Park, Hydrothermal fabrication and characterization of calcium phosphate anhydrous/chitosan composites, Ceram. Int 43 (2) (2017) 2786–2790.
[33] J. Duncan, The role of the chemical composition of monetite on the synthesis and properties of α-tricalcium phosphate, Mater. Sci. Eng. C 34 (2014) 123–129.
[34] O. Kaygili, C. Tatar, S. Keser, N. Bulut, Preparation and characterization of monetites co-doped with Ni/Al, Mater. Lett 201 (2017) 39–42.
[35] L. C. Chow, Solubility of Calcium Phosphates, Octacalcium Phosphate 18 (2001) 94–111.
[36] D. C. Kim, J. H. Kim, J. K. Woo, N. S. Nho, D. H. Shin, R. D. Kaushik, Preparation of Nanofluids of Some Iron Compounds from Industrial Waste FeSO4+ 7H2O as Precursor for NOx Reduction, Asian J. Chem 20 (7) (2008) 5760–5760.
[37] A. Rahmani, H. Z. Mousavi, M. Fazli, Effect of nanostructure alumina on adsorption of heavy metals, Desalination 253 (1-3) (2010) 94–100.
[38] H. Qiu, L. Lv, B. Pan, Q. Zhang, W. Zhang, Q. Zhang, Critical review in adsorption kinetic models, J. Zhejiang Univ.-Sci. A 10 (5) (2009) 716–724.
[39] I. Smičiklas, S. Dimovic, M. Mitrić, Removal of Co2+ from aqueous solutions by hydroxyapatite, Water Res 40 (2006) 2267–74.
[40] A. E. A. Said, Potential Application of Propionic Acid Modified Sugarcane Bagasse for Removing of Basic and Acid Dyes from Industrial Wastewater, Resour. Environ 2 (2012) 93–99.
[41] M. H. Kalavathy, T. Karthikeyan, S. Rajgopal, L. R. Miranda, Kinetic and isotherm studies of Cu(II) adsorption onto H3PO4-activated rubber wood sawdust, J. Colloid Interface Sci 292 (2) (2005) 354–362.
[42] Z. Yaneva, B. Koumanova, S. Allen, Applicability comparison of different kinetic/diffusion models for 4-nitrophenol sorption on Rhizopus oryzae dead biomass, Bulg. Chem. Commun 45 (2013) 161–168.
[43] E. T. Salam, K. M. A. El-Nour, A. A. Awad, A. S. Orabi, Carbon nanotubes modified with 5,7-dinitro-8-quinolinol as potentially applicable tool for efficient removal of industrial wastewater pollutants, Arab. J. Chem 13 (1) (2020) 109–119.
[44] H. M. Baker, A. M. Massadeh, H. A. Younes, Natural Jordanian zeolite: removal of heavy metal ions from water samples using column and batch methods, Environ. Monit. Assess 157 (1) (2009) 319–330.
[45] A. S. Sartape, A. M. Mandhare, P. P. Salvi, D. K. Pawar, S. S. Kolekar, Kinetic and equilibrium studies of the adsorption of Cd(II) from aqueous solutions by wood apple shell activated carbon, Desalination Water Treat 51 (2013) 4638–4650.
[46] S. K. Ponnusamy, R. Subramaniam, S. Kirupha, M. Arukkani, V. Thangaraj, S. Sivanesan, Adsorption behavior of nickel(II) onto cashew nut shell: Equilibrium, thermodynamics, kinetics, mechanism and process design, Chem. Eng. J 167 (2011) 122–131.
[47] A. Olalekan, A. Olatunya, A. O. Dada, Langmuir, Freundlich, Temkin and Dubinin-Radushkevich Isotherms Studies of Equilibrium Sorption of Zn 2+ Unto Phosphoric Acid Modified Rice Husk, J Appl Chem 3 (2012) 38–45.
[48] B. Kwakye-Awuah, B. Sefa-Ntiri, E. Von-Kiti, I. Nkrumah, C. Williams, Adsorptive Removal of Iron and Manganese from Groundwater Samples in Ghana by Zeolite Y Synthesized from Bauxite and Kaolin, Water 11 (9) (2019).
[49] Y. Zhang, J. Zhao, Z. Jiang, S. Dexin, Y. Lu, Biosorption of Fe(II) and Mn(II) Ions from Aqueous Solution by Rice Husk Ash, BioMed Res. Int 2014 (2014) 973095–973095.
[50] A. R. Kaveeshwar, M. Sanders, S. K. Ponnusamy, D. Depan, R. Subramaniam, Chitosan as a biosorbent for adsorption of iron (II) from fracking wastewater, Polym. Adv. Technol 29 (2) (2018) 961–969.
[51] E. Bernard, A. Jimoh, J. Odigure, Heavy metals removal from industrial wastewater by activated carbon prepared from coconut shell, Res J Chem Sci 2231 (2013) 606–606.
[52] S. Banerjee, A. Laminka-Ot, S. R. Joshi, T. Mandal, G. Halder, Optimization of Fe2+ Removal from Coal Mine Wastewater using Activated Biochar of Colocasia esculenta, Water Environ. Res 89 (9) (2017) 774–782.
[53] M. E. Goher, A. M. Hassan, I. A. Abdel-Moniem, A. H. Fahmy, M. H. Abdo, S. M. El-Sayed, Removal of aluminum, iron and manganese ions from industrial wastes using granular activated carbon and Amberlite IR-120H, Egypt. J. Aquat. Res 41 (2) (2015) 155–164.
[54] T. Alslaibi, I. Abustan, M. Azmier, A. Foul, Comparison of Activated Carbon Prepared from Olive Stones by Microwave and Conventional Heating for Iron (II), Environ. Prog. Sustain. Energy 33 (2013).
[55] M. Moghadam, N. Nasirizadeh, Z. Dashti, E. Babanezhad, Removal of Fe(II) from aqueous solution using pomegranate peel carbon: equilibrium and kinetic studies, Int. J. Ind. Chem 4 (2013).